ISBN: 978-628-95207-8-1. ISSN: 2414-6390. Digital Object Identifier: 10.18687/LACCEI2024.1.1.1008

# Design of a Bioinspired Robotic Finger: A Case Study on Conceptual Development for Robotic Hand Applications

Antonio Alberto Jaén Ortega, M.Sc.[1], Maria De Los Angeles Ortega Del Rosario, Ph.D.[2], Per Hellström, Ph.D.[3], Elaine Astrand, Ph.D.[4] and Mikael Ekström Ph.D.[5]
[1,2]Research Group Design, Manufacturing & Materials (DM+M), Universidad Tecnológica de Panamá, Panama City, Panama, antonio.jaenortega@ugent.be, maria.ortega@utp.ac.pa
[2]Centro de Estudios Multidisciplinarios en Ciencia, Ingeniería y Tecnología (CEMCIT-AIP), Panama City, Panama,
[2]Sistema Nacional de Investigación (SNI), Clayton Panama City, Panama
[1]Polymer Chemistry & Biomaterials Research Group, Centre of Macromolecular Chemistry (CMaC), Ghent University, Krijgslaan, Belgium
[3,4,5]Division of Intelligent Future Technologies, Mälardalen University, Sweden, zunh@kth.se, elaine.astrand@mdu.se, mikael.ekstrom@mdu.se

***Abstract*– Human hands and fingers have been widely studied in different fields, such as animation, biomechanics, ergonomics, rehabilitation, medicine, and robotics. However, since the hands are a highly complex part of the human body capable of developing precise tasks, replicating human hand mechanisms remains challenging and, thus, continues to be an active area. This study focuses on a bioinspired mechanically equivalent finger model. A parametric model was proposed based on the typical architecture of a human finger, allowing adaptation to different anthropometries. A forward kinematic model assesses each phalanx's range of motion (ROM) during flexion-extension and abduction-adduction. A CAD modeling technique based on fused filament fabrication (FFF) is used for easy fabrication, requiring no assembly. The resulting model achieves the desired ROM, offering a simple solution for hand modeling. This bioinspired model aids in training hand exoskeleton robots, accurately mimicking human finger mechanics for various applications, including rehabilitation and prosthetics. This model helps understand complex hand mechanisms and holds potential for robotics and related fields.***

***Keywords—hand exoskeleton, design, CAD modeling, additive manufacturing, 3D printing.***

## I. Introduction

Hand motion and gestures, vital for human interaction and functionality, have been extensively researched for decades, impacting diverse fields such as animation, biomechanics, ergonomics, rehabilitation, medicine, and robotics [1], [2], [3], [4], [5]. Achieving digital or prototype hands capable of performing a wide variety of grasps continues to be a key research area. Notably, in fields like rehabilitation, there are significant developments in restoring upper limb function either through the replacement of lost limbs [5] or the use of exoskeletons for activities of daily living (ADLs) [6].

Rehabilitation seeks to restore a person's ability to perform crucial ADLs without assistance [7], [8]. Given that the hand is often the most used body part in executing ADLs, any motion restriction can lead to significant functional loss and, consequently, a diminished quality of life [9].

The upper limbs, especially the hands, are among the most intricate structures in the human body. Located at the extremities of the upper limbs, hands are remarkable for their compact size yet possess a substantial number of degrees of freedom (DOF) and extensive ranges of motion (ROM) [10]. This complexity allows precise movements, such as grasping and manipulating small objects [11]. The effective functioning of hands relies on the harmonious coordination of multiple structures, transforming muscle contractions into functional movements [12]. This intricate process involves the brain sending signals through nerves to the muscles. Tendons then act like a cable-pulley system, working over fulcrums to facilitate movement in unison with the joints. Beyond movement, hands also perform sensory functions; the skin and connective tissues are vital for grip and protection [13]. This sensory feedback is critical, allowing the hand to exert appropriate pressure and fulfill its intended tasks efficiently [12].

In cases where patients are unable to perform ADLs due to conditions such as stroke or cerebral palsy but have not suffered upper limb loss, rehabilitation can benefit from the use of robotics technologies and Industry 4.0 tools. These technologies act as communication systems, interpreting the user's intentions and converting them into commands to control external devices [14], [15], [16]. Such approaches are thought to ease cortical plasticity post-stroke, with research indicating improved motor skills in patients through their application [17]. Thus, a comprehensive understanding of hand motions is crucial to maximize the effectiveness of these rehabilitation technologies [18].

In this study, a mechanically equivalent finger model was explored. This model aims to replicate the Range of Motion (ROM) in a way that allows it to be used as a dummy hand for training an exoskeleton, which is intended for assessing an impaired hand. Consequently, this model's detailed replication of tendinous function is not a primary consideration. These efforts align with the World Health Organization's Rehabilitation 2030: A Call for Action, which emphasizes integrating rehabilitation into universal health systems [24]. This initiative also aligns with Sustainable Development Goal 3, which focuses on ensuring healthy lives and promoting well-being for all ages [18, p. 3].

## II. Biomechanics of the Hand

### A. Anatomy and anthropometry

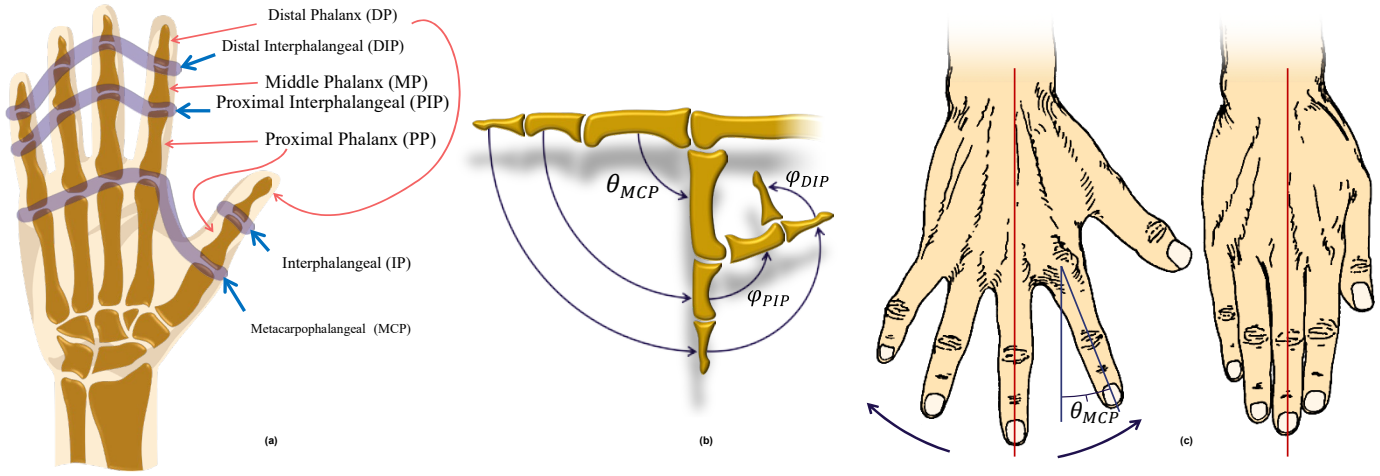


Fig. 1: Morphology and anatomy of the hand: the joints (left) and the phalanxes (right), excluding the palmar and wrist bones (a), ROM during flexion-extension (b) and abduction-adduction (c) motions of the hand, inspired by [12] and [24].

Anatomically, the hands consist of an intricate network of biological structures. This includes 27 bones, 29 skeletal muscles, and 15 joints, as illustrated in Figure 1. Additionally, the hands contain numerous ligaments, tendons, nerves, veins, and other essential components [19], [20]. This complex combination of structures endows the hand with the dexterity required to perform a broad spectrum of activities. Kinematically, this is represented by a model attributing 4 degrees of freedom (DOF) to each finger and 4 or 5 DOF to the thumb, cumulatively amounting to up to 21 degrees of freedom provided by the fingers [21], [22], [23], [24]. This unique and complex anatomy of the human hand facilitates precise movements and a variety of grasping postures.

Without including the wrist bones and except for the thumb, each finger comprises four bones. Starting from the wrist, these bones are the metacarpus, the proximal phalanx (PP), the middle phalanx (MP), and the distal phalanx (DP). The thumb is unique because it does not have the MP (refer to Figure 1 a). Additionally, the hand includes various joints or articulations, which are the connections between the bones. The metacarpophalangeal (MCP) joint is situated between the PP and the metacarpus; the proximal interphalangeal (PIP) joint lies between the PP and the MP; and the distal interphalangeal (DIP) joint is located between the MP and the DP (refer to Figure 1. a). The fingertip (FT) represents the most distal region of the finger.

The metacarpal, PP, and MP can be considered a biarticular bitendinous mechanism chain described by Landsmeer [12], [25]. The tendons act as pulleys, which allow a series of movements and positions together with the joints. This behavior was extensively detailed by [26], where the flexor tendons' excursion is constant and equal to the fully contracted muscle towards the fully extended position. This excursion must be distributed over the three joints so that they can absorb the force required to achieve full-range flexion, as shown in Figure 1.

Furthermore, the joints in the hand can be characterized as follows: The metacarpophalangeal (MCP) joints, which are either ellipsoidal or condylar, possess two DOF, allowing a certain extent of rotational movements. The proximal interphalangeal (PIP) joints are such that an intact volar plate and its control ligaments effectively limit hyperextension. Additionally, the distal interphalangeal (DIP) joints move interdependently with the PIPs. This means that in an extended finger, it is not possible to flex the DIP without also flexing the PIP unless the PIP is locked in extension. This unique behavior is attributed to the presence of an oblique retinacular ligament known as Landsmeer's ligament, which facilitates the transfer of tension between the dorsal aspect of the DIP and the palmar aspect of the PIP [27].

## III. Mechanical Design

The design proposed in this study is that of a finger, drawing bioinspiration from the anatomy and biomechanics of the human hand. It aims to retain enough characteristics to serve as a dummy or training hand for an exoskeleton robot. This robot is designed to produce the necessary force for controlled finger movements and is intended for patients with minimal to no mobility. It will be a wearable, replicable device tailored to fit various hand anthropometries and durable enough to withstand the stresses associated with performing ADLs.

### A. Assumptions

From a biomechanical standpoint, an effective method to categorize the fingers is based on the number of mobile phalanges ($n_{mp}$). This approach groups the fingers into two primary sets: fingers of $n_{mp} = 2$ and fingers of $n_{mp} = 3$. The thumb, with $n_{mp} = 2$, forms its own group, while the index, middle, ring, and pinky fingers, each having $n_{mp} = 3$, comprise the second group. These four fingers are mechanically equivalent in terms of their basic structure, differing only in the dimensions of each phalanx. For the thumb, despite having

fewer phalanges, a similar mechanical model applies, adjusted for the operational characteristics of a finger with $n_{mp} = 2$.

The architecture of each finger consists of phalangeal elements and joints. The joint component pertains to the mechanisms that facilitate movement between the phalanges and between the phalanx and the palm. In contrast, the architecture of the phalanx concerns the solid body structures. The hand possesses phalanges and joints that are equivalent in shape and function among the fingers, albeit with varying dimensions, so the decision was made to start the conceptual design with a single three-phalange finger. This decision was based on the fact that once this finger achieves design maturity, its model can be replicated, accounting for all fingers' conditions accordingly. For instance, the methods employed in 3D modeling the distal phalanges are uniform across different fingers, with alterations only in the variables corresponding to the specific finger being modeled.

### *B. Kinematic analysis*

A kinematic model is proposed to analyze and understand the rotational movements of each phalanx during flexion-extension and abduction-adduction motions of the hand. This comprehensive understanding is crucial for properly training a hand exoskeleton robot. Thus, as a result, this model should detail the range of motion (ROM) for each phalanx, providing valuable insights for its application. In this model, forward kinematics is employed to determine the position of each phalanx (end effector) using known joint angles and dimensions [28]. Euler angles facilitate the transformation of the position vector across reference frames during 3D rotational motion, accurately describing the orientation of a rigid body.

Figure 2 illustrates the kinematic parameters of the finger, detailing the reference frameworks for each phalanx. To conceptualize a joint, it is useful to consider a 'head' and a 'base.' Specifically, for the metacarpophalangeal joint (MCP, denoted as MCPb), the base is situated on the metacarpal bone, indicated by the letter 'M' in Figure 2, and serves as the stationary reference framework. The reference frameworks are positioned at the pivot point at the center of each joint, marked by different colors for clarity: MCP in blue, proximal phalanx (PP) in red, middle phalanx (MP) in purple, and distal phalanx (DP) in mustard. While the lengths of each phalanx are kept constant, the angles vary. The $\theta_{MCP}$ represents the abduction-adduction angle.

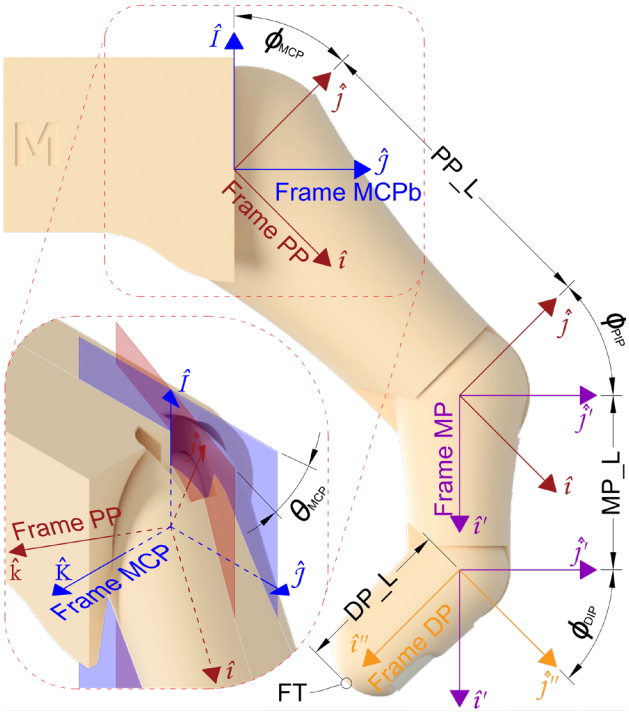


Fig. 1: Kinematic parameters of the finger and the reference frameworks of each phalanx: the MCPb (blue), PP (red), MP (purple), and DP (mustard). The MCP base (MCPb) is set as the fixed reference frame. The $\theta_{MCP}$ represents the abduction-adduction angle.

In equation (1), $\vec{d}_{MCP\cdot FT}$ describes the distance vector between the MCP and the FT, while in equation (2), $\vec{d}_{MCP\cdot DIP}$, describes the distance vector between the MCP and the DIP.

$$\vec{d}_{MCP\cdot FT} = \vec{d}_{MCP\cdot PIP} + \vec{d}_{PIP\cdot DIP} + \vec{d}_{DIP\cdot FT} \quad (1)$$

$$\vec{d}_{MCP\cdot DIP} = \vec{d}_{MCP\cdot PIP} + \vec{d}_{PIP\cdot DIP} \quad (2)$$

Equation (3) depicts the distance vector of the PIP to the MCP, defined with respect to the reference frame PP.

$$\left(\vec{d}_{MCP\cdot PIP}\right)_{PP} = \begin{Bmatrix} PP_L \\ 0 \\ 0 \end{Bmatrix} \quad (3)$$

To analyze the ROM concerning the fixed metacarpophalangeal (MCP) base frame (MCPb), it is necessary to transform this distance from the PP frame to the MCPb frame. This transformation is achieved in equation (4) by multiplying the rotation transformation matrices $[T_Y]_{MCP}$ and $[T_Z]_{MCP}$ which represent rotations about the Y and Z axes in the MCP frame, respectively.

$$\left(\vec{d}_{MCP\cdot PIP}\right)_{MCPb} = [T_Y]_{MCP}[T_Z]_{MCP}\left(\vec{d}_{MCP\cdot PIP}\right)_{PP} \quad (4)$$

These matrices are expressed employing the Eulerian angles in equation (5)

$$[T_Y] = \begin{bmatrix} c_\theta & 0 & -s_\theta \\ 0 & 1 & 0 \\ s_\theta & 0 & c_\theta \end{bmatrix} \quad (5)$$

$$[T_z] = \begin{bmatrix} c_\phi & s_\phi & 0 \\ -s_\phi & c_\phi & 0 \\ 0 & 0 & 1 \end{bmatrix}$$

Where $c_\theta$, and $s_\theta$ are the abbreviations of $\cos\theta$, and $\sin\theta$, respectively. While $c_\varphi$, and $s_\varphi$ are the abbreviations of $\cos\varphi$, and $\sin\varphi$, respectively.

The following distances $\vec{d}_{PIP\cdot DIP}$ and $\vec{d}_{DIP\cdot FT}$ were also expressed regarding their mobile reference frames in equations (6) and (7).

$$\left(\vec{d}_{PIP\cdot DIP}\right)_{MP} = \begin{Bmatrix} MP\_L \\ 0 \\ 0 \end{Bmatrix} \quad (6)$$

$$\left(\vec{d}_{DIP\cdot FT}\right)_{DP} = \begin{Bmatrix} DP\_L \\ 0 \\ 0 \end{Bmatrix} \quad (7)$$

By using the rotation transformation matrices shown in equation (5), these distance vectors can be expressed regarding the fixed reference frame MCPb as shown in equations (8) y (9).

$$\left(\vec{d}_{PIP\cdot DIP}\right)_{MCPb} = [T_Y]_{MCP}[T_Z]_{MCP}[T_Z]_{PIP}\left(\vec{d}_{PIP\cdot DIP}\right)_{MP} \quad (8)$$

$$\left(\vec{d}_{DIP\cdot FT}\right)_{MCPb} = [T_Y]_{MCP}[T_Z]_{MCP}[T_Z]_{PIP}[T_Z]_{DIP}\left(\vec{d}_{DIP\cdot FT}\right)_{DP} \quad (9)$$

### C. Parametric modeling

This study's exploration of hand morphology and functional capabilities guided the approach to replicate its complex mechanism. The aim is not to produce an exact anatomical copy of the hand but to achieve a biomechanical equivalence. To this end, an in-depth examination of biomechanics and control mechanisms was conducted, leading to the conception of a mechanical equivalent model composed of various interconnected parts. Each finger in this model is designed to mimic the natural flexion-extension and abduction-adduction movements observed in human hands, adhering to standard ranges of motion (ROM) [29]. Therefore, every phalanx is treated as a distinct element in this design. The connections between these elements, which correspond to the human hand's DIP, PIP, and IP joints, are proposed to be implemented via a hinge mechanism. This design choice ensures that each joint between the phalanges has a single degree of freedom, closely resembling the functional dynamics of the joints in a human hand.

A ball joint was considered to represent the metacarpophalangeal (MCP) joints in a human hand, which connects the proximal phalanges to the palm. This type of joint permits angular movement with two degrees of freedom (2 DOF), enabling the hand dummy to execute both flexion-extension and abduction-adduction movements of the fingers.

The 3D model of the finger was designed to be customizable to the dimensions of each individual user's hand. Therefore, the model was developed using parameters as variables that represent the measurements of a human hand. A nomenclature system was also proposed to streamline the process of managing the variables necessary for modeling the finger. Each variable consists of three-letter groups: The first group denotes the finger the variable is associated with, the second group identifies the specific phalanx or joint, and the third group indicates the type of dimension the variable represents.

This study aims to develop a mechanical equivalent model of the hand, focusing on biomechanics and control mechanisms rather than creating an exact anatomical replica. This resulted in a multi-part model where each finger can perform flexion-extension and abduction-adduction movements, mirroring the natural range of motion (ROM) observed in human hands [29]. In this model, separate pieces represent each phalanx, with hinge mechanisms simulating the joints (DIP, PIP, and IP) to provide one DOF at each joint. For the metacarpophalangeal (MCP) joints, a ball joint was selected, linking the proximal phalanges to the palm and allowing 2-DOF angular movement, thus enabling the model to replicate the primary motions of the fingers.

To accommodate variations in hand sizes, a customizable 3D finger model was created, integrating parameters that reflect typical human hand measurements. A unique nomenclature for these parameters uses three-letter codes: the first set specifies the finger, the second set identifies the phalanx or joint, and the third set describes the dimension type, ensuring the model's adaptability to individual dimensions.

Manual measurements obtained using a vernier caliper informed the values for the variables represented by *L* (length), *w* (width), and *h* (height) for the customization of the 3D model. These variables correspond to the dimensions of the phalanges and joints, categorized in the second group of the nomenclature. Additionally, variables denoted by the letter A, representing angular measurements, were derived from the findings in references [12] and [27]. Table 1 lists the specific values for the variables Abd (abduction) and A, ensuring the 3D model accurately reflects the unique dimensions of an individual's hand. This method significantly enhances the realism and functionality of the hand dummy across various applications.

Fourteen "L" measurements were recorded to ascertain the length of each phalanx. These lengths involved taking one measurement for each phalanx. To ensure accuracy in measuring the lengths of the proximal (PP) and middle phalanges (MP), it was necessary to place the palm flat against a surface. Measurements were then taken from the center of each joint to the ends of these phalanges. For the distal phalanx (DP), the measurement extended from the center of the distal interphalangeal (DIP) joint to the fingertip.

Additionally, 38 measurements were performed to determine the width ("w") and height ("h") of each joint, with two measurements for each finger joint and two for each fingertip, resulting in a total of 52 manual measurements. These measurements were taken with the fingers fully extended,

carefully placing the vernier caliper on each side of the joint or fingertip for width and from the back of the hand to the palm for height, ensuring no pressure was exerted during measurement.

The measurement of the width of the metacarpophalangeal (MCP) joint presented a unique challenge. Direct measurement was not feasible in a non-invasive manner since the vernier caliper could not be placed on the sides of the MCP. Therefore, an approximate measurement was taken with the palm of the open hand placed on a flat surface, estimating these dimensions on the hand's dorsal (back) side. The resulting measurements are placed in Table 1.

## IV. CAD Modeling of a Single-Finger

This section explains the 3D modeling of the final version of the phalanges and the joints used for the five fingers.

### *A. Phalanges: DP, MP, PP*

The 3D modeling process for the phalanges adopted a uniform approach for all phalanges. as depicted in Figure 3.1 (d), (e), and (f). This approach began with creating the phalangeal body through a loft-type operation using three distinct sketches. The initial and final sketches were designed to reflect the dimensions of the phalanx's corresponding joint sections. The intermediate sketch, placed centrally, served as a mirrored version of the sketch depicting the phalanx's head side. Although a loft operation could technically proceed with merely two sketches, including a central sketch substantially improves the phalanx's final appearance. This addition aids in more accurately mimicking the natural contours of a real finger.

*Table 1: Anthropometry of the fingers. The measurements were collected manually from the subject.*

| Parameters | | | Phalanges | | | Fingertip | | Finger Joints | | | | | | Joint angle ROM (°) | | |
|---|---|---|---|---|---|---|---|---|---|---|---|---|---|---|---|---|
| | | | | | | *FT_* | | *DIP_* | | *PIP_* | | *MCP_* | | *DIP_* | *PIP_* | *MCP_* |
| | | | *DP_L* | *MP_L* | *PP_L* | *w* | *h* | *w* | *h* | *w* | *h* | *w* | *h* | *A* | *A* | *A* |
| **Fingers** | **Index** | **I_** | 21 | 21.5 | 40 | 15 | 12 | 16.5 | 14.6 | 21 | 19 | 19.5 | 28.5 | 90 | 110 | 90 |
| | **Middle** | **M_** | 22.5 | 25 | 45 | 15 | 13.5 | 17 | 15 | 22 | 20.5 | 20 | 32 | 90 | 110 | 90 |
| | **Ring** | **R_** | 21.5 | 21.5 | 39 | 15 | 13.5 | 16 | 14.5 | 20.5 | 19 | 18 | 28.5 | 90 | 110 | 90 |
| | **Pinkie** | **P_** | 20 | 17 | 33 | 13 | 12 | 15 | 14 | 18.5 | 16.5 | 16 | 26 | 90 | 110 | 90 |

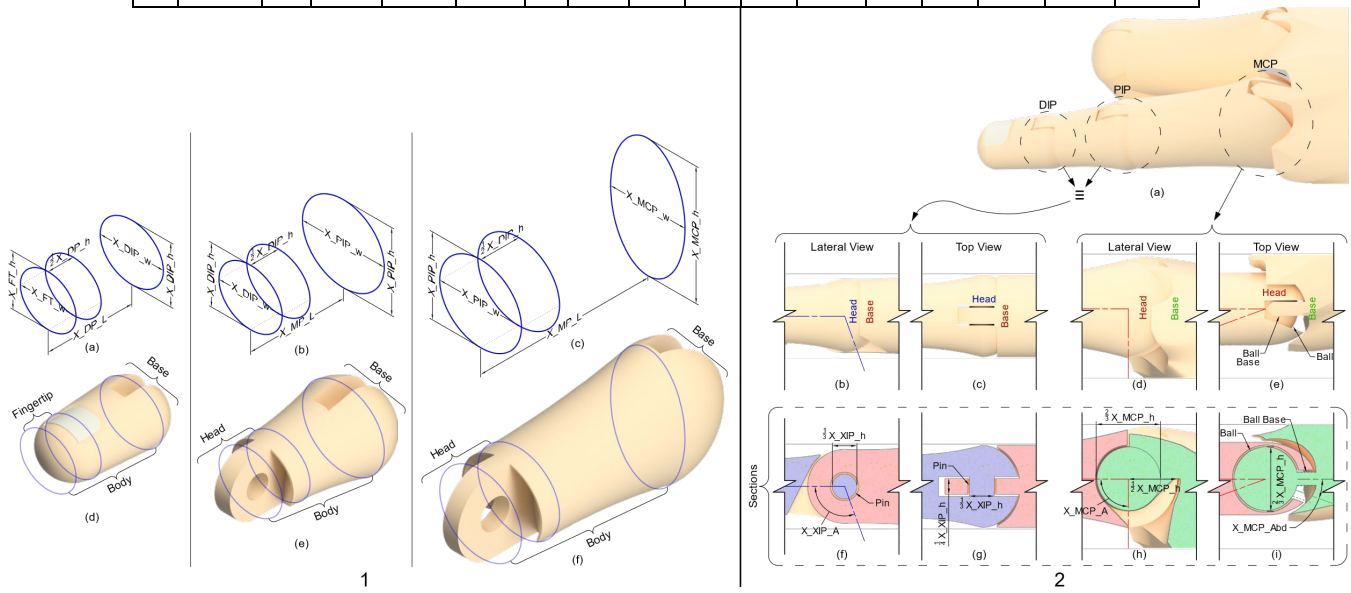


Fig. 2: Finger phalanges and Loft operation sketches to generate (a) the body of the DP. (b) the body of the MP. (c) the body of the PP. (d) Illustration of the PD. (e) MP illustration. (f) PB illustration. In the first letter "X" of the variables used to any finger (T, I, M, R, P).

In modeling the distal phalanx (DP), as illustrated in Figure 3.1 (a) and (d), which are unique in having a single joint at one end, a specific cutting-type revolution operation was employed to achieve a rounded finish, closely simulating the natural curvature of a human finger's tip. To further enhance realism, a nail finish was meticulously added to the fingertip, designed in proportion to the DP's dimensions to ensure an accurate representation of a nail's size relative to the finger. However, it's crucial to acknowledge that the nail finish is intended solely for aesthetic purposes and does not contribute to the model's functional capabilities.

In modeling the distal phalanx (DP) and the proximal phalanx (PP) of the thumb, particular attention was paid to their variable dimensions. For the DP of the thumb, the dimensions at the base section of the model were specifically chosen to match

those of the interphalangeal (IP) joint. Likewise, for the PP of the thumb, the dimensions at the head section are directly derived from the IP joint dimensions.

### *B. Interphalangeal Joints: IP, DIP and PIP*

The IP, DIP, and PIP joints, functioning as hinge joints with a single DOF, are mechanically equivalent. Their 3D modeling used identical operations adjusted for the specific variables of each joint. The design outcomes for the simple hinge mechanism representing these joints are depicted in Figure 3.2 (b), (c), (f), and (g). In the nomenclature, 'X' denotes any of the hand's five fingers, while 'XIP' refers to the joints, applying this approach to model the DIP, PIP, and IP joints due to their shared mechanical system. A minimum clearance of 0.4 mm between the interacting pieces was maintained to ensure mechanical movement without fusion during additive manufacturing, preventing them from behaving as a single rigid body.

This clearance facilitates mechanical movement and is critical for the manufacturing process. The design incorporates a half-spheroid at the ends of the phalanges, granting both the head and base of the phalanges a rounded appearance, matching the size of each joint as shown in Figure 3.1 (a), (b), and (c). As illustrated in Figure 3.2 (f) and (g), space accommodating the pin around which the joint rotates was integrated into the phalanx head design, ensuring the essential 0.4 mm clearance between pieces for unimpeded movement.

To model the base of a phalanx, the design of the previously modeled head was subtracted. This process involved an initial step of duplicating the phalanx head model twice and positioning these duplicates within the target phalanx to establish the base. The duplicates were aligned at the base, with one positioned at the start and the other at the endpoint, considering the joint's range of motion from contraction to extension. An offset of 0.4mm was added to all contact surfaces between the phalanx base and the head models to accommodate for necessary clearance. This ensured a gap for mechanical movement. Following this setup, a combined type of subtraction operation was executed, where the phalanx heads' negative space effectively sculpted the base's shape. Although this modeling approach utilized a cut-type combine operation, similar outcomes could be achieved using a cut-type extrusion technique.

### *C. Metacarpophalangeal joint: MCP*

The ball joint, which was selected as its mechanical equivalent for the metacarpophalangeal (MCP) joint, possesses two DOFs. Although the MCP joint in an actual human hand function as a condyloid joint—characterized by the rounded end of one bone fitting into the concave surface of another—the decision to use a ball joint represents a practical approximation. This simplification, substituting the condyloid joint's complex surfaces with a spheroid-like interface, closely mimics the actual joint's dynamics. Figure 3.2 (d), (e), (h), and (i) showcase the design proposal for an MCP joint that aims to replicate the functionality of a real hand. As with the IP, DIP, and PIP joints, the letter 'X' in the nomenclature denotes any of the hand's five fingers. Consistent with the design strategy for other joints, a minimum clearance of 0.4 mm was maintained between the components to ensure smooth mechanical operation.

Following the modeling of the phalanx base, the process proceeded to the head of the metacarpus, which, in this design, integrates with the hand's stump as a singular piece. Similar to the approach used for the IP, DIP, and PIP joints, the next step involved subtracting solids to create a cavity within the stump's metacarpal base. This cavity is designed to accommodate the finger's proximal phalanx (PP). Subsequently, the components for the hinge ball and its base were crafted, as illustrated in Figure 3.2 (d), (e), (h), and (i), completing the mechanical connection needed for the MCP joint.

## V. Results and analysis

Figure. 4 (a) illustrates the ROMs attainable through the design for the metacarpophalangeal (MIP) joint in red, the proximal interphalangeal (PIP) joint in cyan, and the fingertip (FT) in mustard. The MIP joint is observed to be limited to unidirectional circular motion, reflecting its single DOF. In contrast, the PIP and FT joints demonstrate a broader range of motion, attributed to their 2 DOF and 3 DOF, respectively, allowing for more complex movements. Figure 4 (b) depicts the specific ROM for the FT, focusing on the abduction-adduction movement, which is visualized as a shaded area under the finger. This movement spans a 20° arc to both the right and left, highlighting the design's capability to achieve significant movement volumes within the ROM.

These findings show that the finger design successfully meets the target movement angles and any intermediate positions. While simplifying the intricacies of an actual human finger, the design retains the necessary mobility, employing straightforward geometry. The parameterized design facilitates seamless integration into CAD software, enabling application in diverse fields such as prosthetics and exoskeleton development.

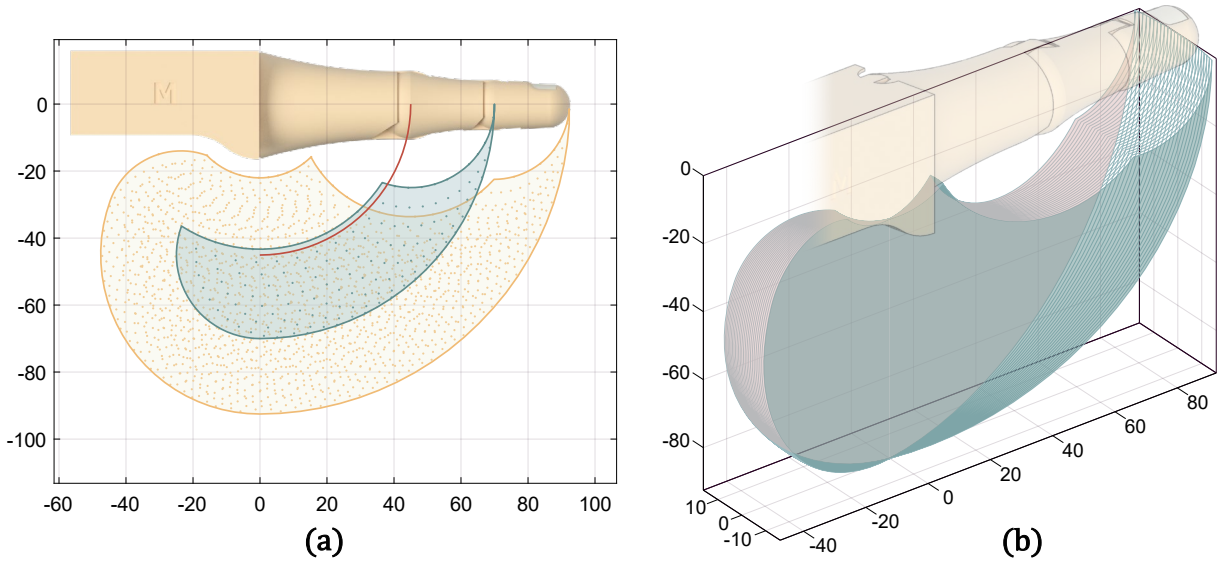


Fig. 3: ROM for an abduction-adduction angle of 0° for: FT (mustard), DIP (cyan), and PIP (red) during flexion-extension motion. The dotted area describes all the positions each joint and the FT reached.

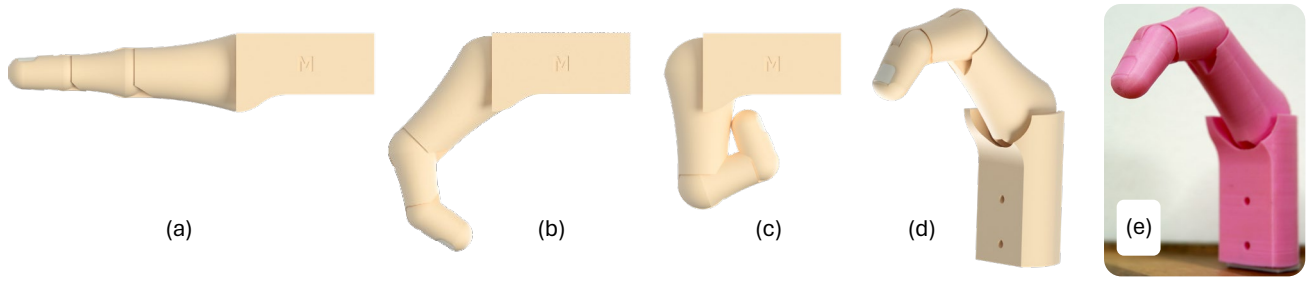


Fig. 4: CAD design for fully extended (a), partially contracted (b), fully contracted finger, rendered image of the finger (d), and additively manufactured bioinspired finger (e).

Furthermore, these results demonstrate the design's capability to achieve the required ROM for a dummy that can be integrated into an exoskeleton and highlight the design's adaptability for single-piece manufacturing via additive manufacturing (FFF). Figure 5 illustrates the opening and closing positions of the fingers (a), (b), and (c), which align with the movements necessary to perform Activities of Daily Living (ADLs), as categorized by the taxonomy proposed by Feix et al. [31] These movements encompass both power and precision, essential for executing ADLs effectively.

As previously outlined, this project aims to manufacture a hand dummy—a mechanically equivalent model that closely mimics a human hand. This allows for the effective training of an exoskeleton without the constant need for patient involvement, thereby eliminating any risk of accidents during the training phase.

Moreover, the design's adherence to the FFF technique throughout its development was a deliberate choice, motivated by the method's accessibility and cost-effectiveness. This approach facilitates a rapid response to personalized design needs and achieves this through the parametric design of the finger, enabling customization to fit various anthropometries. This ensures a tailored response for each individual. Additionally, as depicted in (d) and (e), this finger is manufactured as a single piece, significantly reducing material usage.


## ACKNOWLEDGMENT

The authors would like to thank the Technological University of Panama and the Faculty of Mechanical Engineering (https://fim.utp.ac.pa/, accessed on 10 January 2024) for their collaboration, along with the Research Group on Design, Manufacturing, and Materials. The authors would also like to acknowledge the insightful perspectives of their colleagues on both former and current writings. Furthermore, the authors wish to thank the Secretaría Nacional de Ciencia, Tecnología e Innovación, together with the Sistema Nacional de Investigación (SNI) and the Division of Intelligent Future



**Digital Object Identifier:** (only for full papers, inserted by LACCEI).
**ISSN, ISBN:** (to be inserted by LACCEI).
**DO NOT REMOVE**

Technologies at Mälardalen University, for the partial funding of this project.

## REFERENCES


[1] B. Buchholz y T. J. Armstrong, «A kinematic model of the human hand to evaluate its prehensile capabilities», *Journal of Biomechanics*, vol. 25, n.º 2, pp. 149-162, feb. 1992, doi: 10.1016/0021-9290(92)90272-3.

[2] N. Miyata, M. Kouchi, T. Kurihara, y M. Mochimaru, «Modeling of human hand link structure from optical motion capture data», en *2004 IEEE/RSJ International Conference on Intelligent Robots and Systems (IROS) (IEEE Cat. No.04CH37566)*, sep. 2004, pp. 2129-2135 vol.3. doi: 10.1109/IROS.2004.1389724.

[3] T. M. W. Burton, R. Vaidyanathan, S. C. Burgess, A. J. Turton, y C. Melhuish, «Development of a parametric kinematic model of the human hand and a novel robotic exoskeleton», en *2011 IEEE International Conference on Rehabilitation Robotics*, Zurich: IEEE, jun. 2011, pp. 1-7. doi: 10.1109/ICORR.2011.5975344.

[4] G. Mihalev y S. Yordanov, «Kinematic model and analysis of an anthropomorphic robotic finger», en *2021 International Conference Automatics and Informatics (ICAI)*, sep. 2021, pp. 322-327. doi: 10.1109/ICAI52893.2021.9639774.

[5] J.-M. Boisclair, T. Laliberté, y C. Gosselin, «On the Optimal Design of Underactuated Fingers Using Rolling Contact Joints», *IEEE Robotics and Automation Letters*, vol. 6, n.º 3, pp. 4656-4663, jul. 2021, doi: 10.1109/LRA.2021.3068976.

[6] T. Bützer, O. Lambercy, J. Arata, y R. Gassert, «Fully Wearable Actuated Soft Exoskeleton for Grasping Assistance in Everyday Activities», *Soft Robotics*, vol. 8, n.º 2, pp. 128-143, abr. 2021, doi: 10.1089/soro.2019.0135.

[7] A. M. Dollar, «Classifying Human Hand Use and the Activities of Daily Living», en *The Human Hand as an Inspiration for Robot Hand Development*, R. Balasubramanian y V. J. Santos, Eds., en Springer Tracts in Advanced Robotics. , Cham: Springer International Publishing, 2014, pp. 201-216. doi: 10.1007/978-3-319-03017-3_10.

[8] A. Saudabayev, Z. Rysbek, R. Khassenova, y H. A. Varol, «Human grasping database for activities of daily living with depth, color and kinematic data streams», *Sci Data*, vol. 5, p. 180101, may 2018, doi: 10.1038/sdata.2018.101.

[9] L. Reissner, G. Fischer, R. List, P. Giovanoli, y M. Calcagni, «Assessment of hand function during activities of daily living using motion tracking cameras: A systematic review», *Proc Inst Mech Eng H*, vol. 233, n.º 8, pp. 764-783, ago. 2019, doi: 10.1177/0954411919851302.

[10] T. du Plessis, K. Djouani, y C. Oosthuizen, «A Review of Active Hand Exoskeletons for Rehabilitation and Assistance», *Robotics*, vol. 10, n.º 1, Art. n.º 1, mar. 2021, doi: 10.3390/robotics10010040.

[11] A. B. Ajiboye y R. F. Weir, «Muscle synergies as a predictive framework for the EMG patterns of new hand postures», *J. Neural Eng.*, vol. 6, n.º 3, p. 036004, may 2009, doi: 10.1088/1741-2560/6/3/036004.

[12] Hirt, Bernhard, Harun, Seyhan, Wagner, Michael, y Zumhasch, Rainer, *Hand and Wrist Anatomy and Biomechanics*, Thiemi. India, 2017. Accedido: 1 de mayo de 2022. [En línea]. Disponible en: https://www.thieme.com/books-main/anatomy/product/3967-hand-and-wrist-anatomy-and-biomechanics

[13] T. A. R. Schreuders, J. W. Brandsma, y H. J. Stam, «Functional Anatomy and Biomechanics of the Hand», en *Hand Function*, M. T. Duruöz, Ed., Cham: Springer International Publishing, 2019, pp. 3-21. doi: 10.1007/978-3-030-17000-4_1.

[14] T. Ableitner, S. Soekadar, C. Strobbe, A. Schilling, y G. Zimmermann, «Interaction techniques for a neural-guided hand exoskeleton», *Procedia Computer Science*, vol. 141, pp. 442-446, ene. 2018, doi: 10.1016/j.procs.2018.10.164.

[15] M. A. Khan, R. Das, H. K. Iversen, y S. Puthusserypady, «Review on motor imagery based BCI systems for upper limb post-stroke neurorehabilitation: From designing to application», *Computers in Biology and Medicine*, vol. 123, p. 103843, ago. 2020, doi: 10.1016/j.compbiomed.2020.103843.

[16] M. Zhuralvev, A. Runnova, y A. Kiselev, «Characteristics of post-stroke patients brain activity with real and imagined movements in the BCI - rehabilitation process», *Procedia Computer Science*, vol. 169, pp. 677-685, ene. 2020, doi: 10.1016/j.procs.2020.02.184.

[17] N. A. Bhagat *et al.*, «Neural activity modulations and motor recovery following brain-exoskeleton interface mediated stroke rehabilitation», *NeuroImage: Clinical*, vol. 28, p. 102502, ene. 2020, doi: 10.1016/j.nicl.2020.102502.

[18] A. A. Jaén Ortega, M. Ortega Del Rosario, P. Hellström, E. Åstrand, y M. Ekström, «On Understanding the Role of Exoskeleton Robots in Hand Rehabilitation: A Brief Review», en *2022 8th International Engineering, Sciences and Technology Conference (IESTEC)*, oct. 2022, pp. 432-439. doi: 10.1109/IESTEC54539.2022.00074.

[19] R. L. Drake, W. Vogl, A. W. M. Mitchell, y H. Gray, *Gray's anatomy for students*. 2015.

[20] O. Luhmann, «Development of a Novel Hand Exoskeleton for the Rehabilitation and Assistance of Upper Motor Neuron Syndrome Patients», p. 129, 2020.

[21] M. V. Arteaga, J. C. Castiblanco, I. F. Mondragon, J. D. Colorado, y C. Alvarado-Rojas, «EMG-driven hand model based on the classification of individual finger movements», *Biomedical Signal Processing and Control*, vol. 58, p. 101834, abr. 2020, doi: 10.1016/j.bspc.2019.101834.

[22] R. A. R. C. Gopura, D. S. V. Bandara, K. Kiguchi, y G. K. I. Mann, «Developments in hardware systems of active upper-limb exoskeleton robots: A review», *Robotics and Autonomous Systems*, vol. 75, pp. 203-220, ene. 2016, doi: 10.1016/j.robot.2015.10.001.

[23] M. A. Rahman y A. Al-Jumaily, «Design and Development of a Hand Exoskeleton for Rehabilitation Following Stroke», *Procedia Engineering*, vol. 41, pp. 1028-1034, 2012, doi: 10.1016/j.proeng.2012.07.279.

[24] M. Zarzoura, P. del Moral, M. I. Awad, y F. A. Tolbah, «Investigation into reducing anthropomorphic hand degrees of freedom while maintaining human hand grasping functions», *Proc Inst Mech Eng H*, vol. 233, n.º 2, pp. 279-292, feb. 2019, doi: 10.1177/0954411918819114.

[25] J. M. F. Landsmeer, *Atlas of anatomy of the hand / by Johan M. F. Landsmeer.* Edinburgh ; New York: Churchill Livingstone, 1976.

[26] E. A. Zancolli y E. P. Cozzi, *Atlas of Surgical Anatomy of the Hand*. New York, 1992.

[27] R. J. Smith, «Balance and kinetics of the fingers under normal and pathological conditions», *Clin Orthop Relat Res*, n.º 104, pp. 92-111, oct. 1974, doi: 10.1097/00003086-197410000-00010.

[28] M. B. Popovic y M. P. Bowers, «2 - Kinematics and Dynamics», en *Biomechatronics*, M. B. Popovic, Ed., Academic Press, 2019, pp. 11-43. doi: 10.1016/B978-0-12-812939-5.00002-1.

[29] S. Cobos, M. Ferre, M. A. Sanchez Uran, J. Ortego, y C. Pena, «Efficient human hand kinematics for manipulation tasks», en *2008 IEEE/RSJ International Conference on Intelligent Robots and Systems*, sep. 2008, pp. 2246-2251. doi: 10.1109/IROS.2008.4651053.

[30] S. Hoppenfeld y R. Hutton, *Physical examination of the spine and extremities*. New York: Appleton-Century-Crofts, 1976.

[31] T. Feix, J. Romero, H.-B. Schmiedmayer, A. M. Dollar, y D. Kragic, «The GRASP Taxonomy of Human Grasp Types», *IEEE Transactions on Human-Machine Systems*, vol. 46, n.º 1, pp. 66-77, feb. 2016, doi: 10.1109/THMS.2015.2470657.